ASTEROID ORBITS WITH GAIA: INVERSION AND PREDICTION

Karri Muinonen, Jenni Virtanen, Mikael Granvik, Teemu Laakso

Observatory, P.O. Box 14, FI-00014 University of Helsinki, Finland

ABSTRACT

We present numerical methods for the inversion of forthcoming Gaia astrometry for asteroid orbital-element probability density functions. In the initial orbit computation for two or more observations, the statistical ranging technique (Ranging) allows a Monte Carlo (MC) sampling of the phase space of the orbital elements. In assessing the rapidly improving orbits in what we call the phase-transition regime, we sample the phase-space volumes of variation with the help of local linear approximations along the lines of variation (VOV sampling). For extensively observed asteroids, the standard linear approximation based on nonlinear least squares provides the differentially corrected orbital elements and their covariance matrices based on partial derivatives. We offer a short theoretical treatment of the linking and identification problems, that is, the problems of linking different observation sets and cross-identifying objects in the sets. Here we describe the general concepts of the socalled address comparison techniques that entail a one-dimensional discretization for phase spaces of arbitrary dimension. We summarize the current state of the Fortran95 software developed for the Gaia orbital inverse and linking problems and, in a companion article, apply the methods to simulated Gaia astrometry.

Key words: Gaia; Asteroids; NEOs; Asteroid orbit computation; Asteroid identification; Inverse problems.

1. INTRODUCTION

Gaia promises to provide astrometry of revolutionary accuracy for large numbers of small Solar System bodies crossing the near-Earth space (NEOs, near-Earth objects), asteroids residing in the main belt between Mars and Jupiter (MBOs, main-belt objects), and Jupiter Trojan, Centaur, and transneptunian objects orbiting the Sun in more distant space. Gaia will additionally detect a number of comets and natural satellites of planets. All of the small bodies give rise to inverse problems of deriving orbital-element probability density functions (p.d.f.'s) from the astrometric observations by Gaia. In what follows, we provide the theoretical methods currently applicable to asteroid orbit computation.

The recent progress in asteroid orbit computation is reviewed by Bowell et al. (2002). Here we summarize certain advances in orbit computation from the last decade or so. What has led to these advances is the increased demand on the accuracy of asteroid orbit computation, via the realization that NEOs constitute a significant risk for the prosperity and survival of the human species. The orbit computation techniques have been accompanied by techniques for close approach and collision probability assessment (Milani et al. 2002).

The present paper is the first of two papers assessing asteroid orbit computation using forthcoming Gaia astrometry. Here we provide a detailed description of the theoretical methods involved in interpreting the Gaia data, whereas in the companion paper (Virtanen et al. 2005) the techniques are applied to a number of example cases arising from simulated Gaia data. We emphasize that the global solution for asteroid orbits from Gaia data will only be ready at the end of the survey, because the asteroid dynamical evolution and physical properties are intertwined due to the precision of the Gaia astrometry. The full statistical inverse problem encompasses solving for the sizes, shapes and masses (also for perturbing objects) as well as relativistic effects simultaneously for large numbers of asteroids[1].

In Section 2, we summarize the *a posteriori* p.d.f. for orbital elements, and the various techniques to characterize the p.d.f. In Section 3, we provide a treatment of the statistical techniques for linking different observations and identifying objects. Section 4 assesses the current orbit computation software, briefly summarizing the capabilities and limitations. We conclude the paper by outlining future prospects in Section 5.

2. INVERSE PROBLEM

2.1. Orbital-element Probability Density

Assume that N pairs of positions in Gaia-centric longitude and latitude $\psi = (\lambda_1, \beta_1; \ldots; \lambda_N, \beta_N)^T$ have been observed for a certain asteroid at times $t = (t_1, \ldots, t_N)^T$

---

[1] see http://www.obs-nice.fr/tanga/SSWG/ – the web site of the Gaia Solar System Working Group

(T stands for transpose). Here it is formally straight-forward to include motions in longitude and latitude ($\dot{\lambda}$ and $\dot{\beta}$) as observables.

Let the theoretical, computed light–time–corrected sky–plane positions be described by the vector $\boldsymbol{\Psi}(\boldsymbol{P})$ for the osculating orbital elements $\boldsymbol{P}$ of an asteroid at a given epoch t_0. For Keplerian elements, $\boldsymbol{P} = (a, e, i, \Omega, \omega, M_0)^T$ (T is transpose) and the elements are, respectively, the semimajor axis, eccentricity, inclination, longitude of ascending node, argument of perihelion, and mean anomaly. The three angular elements i, Ω, and ω are currently referred to the ecliptic at equinox J2000.0. For Cartesian elements, $\boldsymbol{P} = (X, Y, Z, \dot{X}, \dot{Y}, \dot{Z})^T$ where, in a given Cartesian reference frame, the coordinates $(X, Y, Z)^T$ denote the position and the coordinates $(\dot{X}, \dot{Y}, \dot{Z})^T$ the velocity.

The astrometric observations, theoretical positions, and observational errors are related to each other through the observation equation,

$$\Delta\boldsymbol{\psi} = \boldsymbol{\psi} - \boldsymbol{\Psi}(\boldsymbol{P}) = \boldsymbol{\epsilon}$$
$$\boldsymbol{\epsilon} = (\epsilon_{\alpha 1}, \epsilon_{\delta 1}; \ldots ; \epsilon_{\alpha N}, \epsilon_{\delta N})^T, \quad (1)$$

where the vector $\boldsymbol{\epsilon}$ describes the observational errors assumed to be drawn from an observational error p.d.f.

The orbital-element p.d.f. p_p is proportional to the *a priori* (p_pr) and observational error p.d.f.'s (p_ϵ), the latter being evaluated for the sky-plane ('Observed-Computed' or 'O-C') residuals $\Delta\boldsymbol{\psi}(\boldsymbol{P})$ (Muinonen & Bowell 1993),

$$p_\mathrm{p}(\boldsymbol{P}) \propto p_\mathrm{pr}(\boldsymbol{P})p_\epsilon(\Delta\boldsymbol{\psi}(\boldsymbol{P})), \quad (2)$$

where p_ϵ can usually be assumed to be Gaussian. For the mathematical form of p_p to be invariant in transformations from one orbital element set to another (e.g., from Keplerian to equinoctial or Cartesian), we regularize the statistical analysis by Jeffreys' noninformative *a priori* p.d.f. (Jeffreys 1946; see also Muinonen et al. 2001),

$$p_\mathrm{pr}(\boldsymbol{P}) \propto \sqrt{\det\Sigma^{-1}(\boldsymbol{P})},$$
$$\Sigma^{-1}(\boldsymbol{P}) = \Phi(\boldsymbol{P})^T\Lambda^{-1}\Phi(\boldsymbol{P}), \quad (3)$$

where Σ^{-1} is the information matrix (or the inverse covariance matrix) evaluated for the orbital elements $\boldsymbol{P}$, Φ contains the partial derivatives of right ascension (R.A.) and declination (Dec.) with respect to the orbital elements, and Λ is the covariance matrix for the observational errors. By the choice of the *a priori* p.d.f., the transformation of rigorous p.d.f.'s becomes analogous to that of Gaussian p.d.f.'s.

The final *a posteriori* orbital-element p.d.f. is, with the help of the χ^2 evaluated for the elements $\boldsymbol{P}$,

$$p_\mathrm{p}(\boldsymbol{P}) \propto \sqrt{\det\Sigma^{-1}(\boldsymbol{P})} \exp\left[-\frac{1}{2}\chi^2(\boldsymbol{P})\right],$$
$$\chi^2(\boldsymbol{P}) = \Delta\boldsymbol{\psi}^T(\boldsymbol{P})\Lambda^{-1}\Delta\boldsymbol{\psi}(\boldsymbol{P}). \quad (4)$$

As a consequence of securing the invariance in orbital-element transformations, e.g., ephemeris uncertainties and collision probabilities based on the orbital-element

p.d.f. are independent of the choice of the orbital element set. Note that assuming constant p_pr is acceptable, when the exponent part of Equation 4 confines the p.d.f. into a phase-space regime, where the determinant part reduces to a constant.

2.2. Linear Approximation

In the validity regime of the linear approximation,

$$\chi^2(\boldsymbol{P}) \approx \chi^2(\boldsymbol{P}_\mathrm{ls}) + \Delta\boldsymbol{P}^T\Sigma^{-1}(\boldsymbol{P}_\mathrm{ls})\Delta\boldsymbol{P},$$
$$\Delta\boldsymbol{P} = \boldsymbol{P} - \boldsymbol{P}_\mathrm{ls},$$
$$\det\Sigma^{-1}(\boldsymbol{P}) \approx \det\Sigma^{-1}(\boldsymbol{P}_\mathrm{ls}), \quad (5)$$

where $\boldsymbol{P}_\mathrm{ls}$ denotes the least-squares orbital elements. The resulting orbital-element p.d.f. is Gaussian,

$$p_\mathrm{p}(\boldsymbol{P}) \propto \sqrt{\det\Sigma^{-1}(\boldsymbol{P}_\mathrm{ls})} \cdot$$
$$\exp\left[-\frac{1}{2}\Delta\boldsymbol{P}^T\Sigma^{-1}(\boldsymbol{P}_\mathrm{ls})\Delta\boldsymbol{P}\right]. \quad (6)$$

The least-squares orbital elements $\boldsymbol{P}_\mathrm{ls}$ and their covariance matrix Σ constitute the full, concise solution to the inverse problem in the linear approximation.

The linear approximation follows from the solution of the inverse problem via differential corrections, expressed in the following iterative way:

$$\boldsymbol{P}_\mathrm{ls} \leftarrow \boldsymbol{P}_\mathrm{ls} + \left[\Phi^T(\boldsymbol{P}_\mathrm{ls})\Lambda^{-1}\Phi(\boldsymbol{P}_\mathrm{ls})\right]^{-1} \cdot$$
$$\Phi^T(\boldsymbol{P}_\mathrm{ls})\Lambda^{-1}\Delta\boldsymbol{\psi}(\boldsymbol{P}_\mathrm{ls})$$
$$\begin{cases} \Phi_{2k-1,j} = \cos\beta_k \frac{\partial\lambda}{\partial P_j}(\boldsymbol{P}_\mathrm{ls}, t_k), \\ \Phi_{2k,j} = \frac{\partial\beta}{\partial P_j}(\boldsymbol{P}_\mathrm{ls}, t_k), \end{cases}$$
$$k = 1, 2, 3, \ldots, N. \quad (7)$$

Upon convergence, the differential correction procedure yields the nonlinear least-squares solution of the orbital elements. The covariance matrix of the elements follows in a linear approximation in the proximity of the least-squares orbital elements,

$$\Sigma(\boldsymbol{P}_\mathrm{ls}) = \left[\Phi^T(\boldsymbol{P}_\mathrm{ls})\Lambda^{-1}\Phi(\boldsymbol{P}_\mathrm{ls})\right]^{-1}. \quad (8)$$

The strict linear approximation would involve the simultaneous linearization of the exponential and determinant parts of the rigorous *a posteriori* p.d.f. Although computationally accessible, first, the strict linearization would result in the abandonment of the commonly used differential correction procedure to obtain the best-fit orbit and, second, would introduce second-order partial derivatives into the search for the orbital elements at the tip of the a posteriori p.d.f. Sacrificing some of the mathematical rigor, without an effect on the accuracy of the results following, we adopt the more practical definition for the linear approximation in Equation 5.

2.3. Volume-of-Variation Sampling

The *a posteriori* p.d.f. in Equation 4 allows the derivation of a local linear approximation in the orbital-element

phase space (Muinonen et al. 2004, Virtanen & Muinonen 2004). We can select one or more elements as 'the elements to be varied' systematically and derive a linear approximation for 'the remaining elements to be fitted'. For simplicity, we illustrate the local linear approximations below in the case of a single mapping element and note that the formulation is analogous for more numerous mapping elements.

We rewrite the *a posteriori* p.d.f. in Equation 4 explicitly in terms of the mapping element $P_{\rm m}$ and the five remaining elements $\boldsymbol{P}'$ (here and below, the prime denotes five-dimensional quantities),

$$
\begin{aligned}
p_{\rm p}(P_{\rm m}, \boldsymbol{P}') &\propto \sqrt{\det \Sigma^{-1}(P_{\rm m}, \boldsymbol{P}')} \cdot \\
&\qquad \exp\left[-\frac{1}{2}\chi^2(P_{\rm m}, \boldsymbol{P}')\right], \\
\chi^2(P_{\rm m}, \boldsymbol{P}') &= \Delta\boldsymbol{\psi}^T(P_{\rm m}, \boldsymbol{P}')\Lambda^{-1}\Delta\boldsymbol{\psi}(P_{\rm m}, \boldsymbol{P}') \quad (9)
\end{aligned}
$$

For a given $P_{\rm m}$, we define the local linear approximation as follows,

$$
\begin{aligned}
p_{\rm p}(P_{\rm m}, \boldsymbol{P}') &\propto \sqrt{\det \Sigma^{-1}(P_{\rm m}, \boldsymbol{P}'_{\rm ls})} \cdot \\
&\qquad \exp\left[-\frac{1}{2}\chi^2(P_{\rm m}, \boldsymbol{P}'_{\rm ls})\right] \cdot \\
&\qquad \exp\left[-\frac{1}{2}\Delta\boldsymbol{P}'^T\Sigma'^{-1}(P_{\rm m}, \boldsymbol{P}'_{\rm ls})\Delta\boldsymbol{P}'\right], \\
\Delta\boldsymbol{P}' &= \boldsymbol{P}' - \boldsymbol{P}'_{\rm ls}(P_{\rm m}), \quad (10)
\end{aligned}
$$

where $\boldsymbol{P}'_{\rm ls} = \boldsymbol{P}'_{\rm ls}(P_{\rm m})$ is the local least-squares solution for the elements $\boldsymbol{P}'$. Note that both Σ^{-1} and Σ'^{-1} enter the local linear approximations above. The sequence of orbital elements $P_{\rm m}, \boldsymbol{P}'_{\rm ls}(P_{\rm m})$ defines the line of variation in the orbital-element phase space.

The local covariance matrix Σ' defines a hyperellipsoid centred at the local least-squares orbital elements (cf. Muinonen 1996),

$$
\Delta\chi^2(\boldsymbol{P}') = \Delta\boldsymbol{P}'^T\Sigma'^{-1}\Delta\boldsymbol{P}' = \Delta\chi_0^2, \quad (11)
$$

where $\Delta\chi_0^2$ is a constant. The boundaries of, for example, the commonly used 68.3% or 95.4% -probability hyperellipsoids are $\Delta\chi_0^2 \approx 5.89$ or $\Delta\chi_0^2 \approx 11.3$, respectively.

It is convenient to express the differences $\Delta\boldsymbol{P}'$ in terms of the standard deviations $\sigma'_j = \sqrt{\Sigma'_{jj}}$ $(j = 1, \ldots, 5)$ and to utilize the dimensionless correlation matrix C'; with the help of the diagonal standard deviation matrix S',

$$
\begin{aligned}
\Delta\boldsymbol{Q}' &= S'^{-1}\Delta\boldsymbol{P}', \\
C' &= S'^{-1}\Sigma'S'^{-1}, \\
S'_{jk} &= \sigma'_j \delta_{jk}, \quad j, k = 1, \ldots, 6, \quad (12)
\end{aligned}
$$

where δ_{jk} is the Kronecker symbol. The hyperellipsoid is thus defined by

$$
\Delta\boldsymbol{Q}'^T C'^{-1}\Delta\boldsymbol{Q}' = \Delta\chi_0^2, \quad (13)
$$

where all the parameters are dimensionless. The eigenvalues λ'_j $(j = 1, \ldots, 5)$ for the correlation matrix C' are normalized variances along the principal axes of the hyperellipsoid, the directions of the axes being given by the orthonormal eigenvectors $\boldsymbol{X}'_j$,

$$
C'\boldsymbol{X}'_j = \lambda'_j\boldsymbol{X}'_j, \quad j = 1, \ldots, 5. \quad (14)
$$

Since C' is a real and symmetric matrix, the eigenproblem is readily solved via Jacobi transformations (Press et al. 1994).

Once the eigenvalues and eigenvectors are available, the shape and orientation of the hyperellipsoid become transparent. For example, points on the hypersurface in the directions of the principal axes corresponding to a given $\Delta\chi_0^2$ are

$$
\begin{aligned}
\boldsymbol{P}'^{\pm}_j &= \boldsymbol{P}'_{\rm ls} \pm \sqrt{\Delta\chi_0^2\,\lambda'_j}S'\boldsymbol{X}'_j, \\
&\qquad j = 1, \ldots, 5. \quad (15)
\end{aligned}
$$

The local linear approximations allow the study of the validity of the global linear approximation: if the local least-squares solutions do not fall on a straight line or if the local covariances differ, the global linear approximation must be rejected. The covariance matrix differences can be measured using, for example, the L^2 metric for matrices, that is, summing the squares of the matrix element differences.

On one hand, the straightforward application of the local linear approximations suffers from shortcomings: it requires the storage of large numbers (several hundreds to thousands) of mapping elements, covariance matrices, and weight factors, without certainty of validity across the regime studied for the mapping element. On the other hand, as shown below, the local linear approximations can constitute an invaluable guide, in the orbital-element phase space, to the proximity of orbit solutions for the rigorous inverse problem.

The validity of the local linear approximations depends on the set of orbital elements selected. Whereas Keplerian elements are attractive because of their conceptual clarity, Cartesian elements can in general be preferable. We can offer the following reasoning based on Gaussian random variables to support a choice of a certain Cartesian set of orbital elements. Select an epoch for the orbital elements coinciding with one of the observation dates close to the mid-point of the observational time arc. Consider then orbital elements that are the Cartesian position vector $(X, Y, Z)^T$ and velocity vector $(\dot{X}, \dot{Y}, \dot{Z})^T$, where the z-axis points in the topocentric direction of the object and the x and y axes coincide with the R.A. and Dec. axes, respectively. In particular, for exiguous observational data, the potential Gaussian characteristics of the four transverse orbital elements $(X, Y)^T$ and $(\dot{X}, \dot{Y})^T$ are suggested by the sum rule for Gaussian random variables: adding or subtracting Gaussian random variables results in random variables that are Gaussian. Here $(X, Y)^T$ and $(\dot{X}, \dot{Y})^T$ can be taken as rough estimates of the mean position and position differences on the sky plane. Thus, the two natural mapping elements are the line-of-sight distance (range) and velocity (radial velocity or range rate) of the object at the given epoch.

It is our goal to draw sample orbits from the rigorous orbital-element p.d.f. with the help of the local linear approximations. First, we specify the variation interval for the mapping element with the help of the covariance matrix Σ derived in the global linear approximation and emphasize that the variation interval must be subject to iteration. For example, one may utilize the one-dimensional 3σ variation interval as given by the linear approximation so that

$$P_{\mathrm{m}} \in [P_{\mathrm{m,ls}} - 3\sigma_{\mathrm{m}}, P_{\mathrm{m,ls}} + 3\sigma_{\mathrm{m}}], \qquad (16)$$

where $P_{\mathrm{m,ls}}$ is the global least-squares value for the mapping element. Second, the remaining elements are sampled with the help of the local intervals of variation so that

$$\boldsymbol{P}' = \boldsymbol{P}'_{\mathrm{ls}}(P_{\mathrm{m}}) + \sum_{j=1}^{5} (1 - 2r_j) \cdot$$
$$\sqrt{\Delta\tilde{\chi}^2 \lambda'_j(P_{\mathrm{m}})} S'(P_{\mathrm{m,ls}}) \boldsymbol{X}'_j(P_{\mathrm{m}}), \quad (17)$$

where $r_j \in (0,1)$ $(j = 1, \ldots, 5)$ are independent uniform random deviates and $\Delta\tilde{\chi}^2$ is a scaling parameter to be iterated so that the entire orbit solution space is covered and the final results have converged. Initially, one may start with $\Delta\tilde{\chi}^2 = 11.3$ and slowly increase its value. $S'(P_{\mathrm{m,ls}})$ designates the single standard deviation matrix used throughout the interval of the mapping parameter, which allows a straightforward debiasing of the sample orbits at the end of the computation. Here, $S'(P_{\mathrm{m,ls}})$ is the S' matrix evaluated at the global least-squares value of the mapping element P_{m}.

In Equation 17, we sample the local phase-space volume using the principal-axis directions following from the local linear approximation, after diagonalization by the solution of the eigenproblem in the units specified by the S' matrix. In the present context, the shape of the local sampling volume is that of a five-dimensional rectangular parallelepiped.

In practical computations, we need to discretize the interval of the mapping element and, after solving the five-dimensional local least-squares problem, interpolate the interval parameters for Equation 17.

Once the entire variation-interval map is available across the interval of the mapping parameter, trial orbits are generated in a straightforward way. First, a value for the mapping orbital element is obtained from uniform sampling over the mapping interval. Second, the remaining five elements are generated by interpolating their variation intervals based on the precomputed map. Third, the trial orbit qualifies for a sample orbit if it produces an acceptable fit to the observations. Each sample orbit is accompanied by the weight factor

$$w(P_{\mathrm{m}}, \boldsymbol{P}') \propto \sqrt{\det \Sigma^{-1}(P_{\mathrm{m}}, \boldsymbol{P}')} \cdot$$
$$\exp\left[-\frac{1}{2}\chi^2(P_{\mathrm{m}}, \boldsymbol{P}')\right] \cdot$$
$$\sqrt{\frac{\lambda_1(P_{\mathrm{m}}) \cdot \ldots \cdot \lambda_5(P_{\mathrm{m}})}{\lambda_1(P_{\mathrm{m,ls}}) \cdot \ldots \cdot \lambda_5(P_{\mathrm{m,ls}})}}. (18)$$

The local linear approximations allow the generation of trial orbits using the five-dimensional Gaussian p.d.f.'s. In Equation 17, such an alternative approach would entail the replacement of the uniform random deviate factors $(1 - 2r_j)$ by Gaussian deviates, and would result in an additional debiasing Gaussian p.d.f. divisor in Equation 18. Such an approach results in larger numbers of sample orbits close to the line of variation, which can be desirable in cases of heavy computational burden. But, simultaneously, less attention would be paid to the potential solutions further away from the line of variation. In the limit of large numbers of sample orbits, the two approaches yield identical results.

Because of the noninformative *a priori* p.d.f., results from VOV sampling are invariant in orbital-element transformations. The choice of the orbital element set is, however, nontrivial as assessed in Section 2.2: the computational speed and applicability of VOV depend on the validity of the local linear approximations as a function of the mapping element.

2.4. Statistical Orbital Ranging

For initial orbit computation using Gaia data, we make use of Ranging (Virtanen et al. 2001, Muinonen et al. 2001). In Ranging, two observation dates (here A and B) are chosen from the complete observation set. The corresponding Gaia-centric distances (or ranges R_{A} and R_{B}), as well as the longitudes (λ_{A} and λ_{B}) and latitudes (β_{A} and β_{B}) are MC sampled using intervals subject to iteration, resulting in altogether 12 interval boundary parameters. Explicitly,

$$\begin{cases} R_{\mathrm{A}} & \in [R_{\mathrm{A}}^-, R_{\mathrm{A}}^+], \\ \lambda_{\mathrm{A}} & \in [\lambda_{\mathrm{A}}^-, \lambda_{\mathrm{A}}^+], \\ \beta_{\mathrm{A}} & \in [\beta_{\mathrm{A}}^-, \beta_{\mathrm{A}}^+], \end{cases}$$
$$\begin{cases} R_{\mathrm{B}} & \in [R_{\mathrm{A}} + R_{\mathrm{B}}^-, R_{\mathrm{A}} + R_{\mathrm{B}}^+], \\ \lambda_{\mathrm{B}} & \in [\lambda_{\mathrm{A}}^-, \lambda_{\mathrm{A}}^+], \qquad (19) \\ \beta_{\mathrm{B}} & \in [\beta_{\mathrm{A}}^-, \beta_{\mathrm{A}}^+]. \end{cases}$$

Note that it is computationally efficient to generate R_{B} based on R_{A} generated at an earlier stage. The boundary values $R_{\mathrm{B}}^{\pm}$ must be carefully chosen so as to secure the coverage of the entire relevant interval in R_{B}.

Once the two sets of spherical coordinates have been generated, the two corresponding Cartesian positions $(X_{\mathrm{A}}, Y_{\mathrm{A}}, Z_{\mathrm{A}})^T$ and $(X_{\mathrm{B}}, Y_{\mathrm{B}}, Z_{\mathrm{B}})^T$ lead to an unambiguous set of orbital elements $\boldsymbol{P}$, based on well-established techniques in celestial mechanics (Danby 1992).

The set of trial orbital elements $\boldsymbol{P}$ is included in the set of sample orbital elements if and only if it produces an acceptable fit to the entire set of observations, that is, with the help of Equation 4,

$$\exp\left[-\frac{1}{2}(\chi^2(\boldsymbol{P}) - \chi^2(\boldsymbol{P}_{\mathrm{ref}})) + \right.$$
$$\left. \ln\sqrt{\det \Sigma^{-1}(\boldsymbol{P})} - \ln\sqrt{\det \Sigma^{-1}(\boldsymbol{P}_{\mathrm{ref}})} \right]$$
$$\geq c_{\min}, \qquad (20)$$

where $c_{\min}$ is the level of acceptance and $\boldsymbol{P}_{\mathrm{ref}}$ refers to the best-fit orbital solution available, constantly updated during the iterative computation. The acceptance criterion thus becomes analogous to the $\Delta\chi^2$ criterion for Gaussian p.d.f.'s (Equation 11).

In order to establish the uniform sampling of orbital elements $\boldsymbol{P}$, each set of sample orbital elements is weighted by the Jacobian of the transformation from 'the phase space' of the two spherical positions $(R_{\mathrm{A}}, \lambda_{\mathrm{A}}, \beta_{\mathrm{A}})^T$ and $(R_{\mathrm{B}}, \lambda_{\mathrm{B}}, \beta_{\mathrm{B}})^T$ to the phase space of the orbital elements,

$$w(\boldsymbol{P}) \quad \propto \quad \det\left[\frac{\partial(R_{\mathrm{A}}, \lambda_{\mathrm{A}}, \beta_{\mathrm{A}}; R_{\mathrm{B}}, \lambda_{\mathrm{B}}, \beta_{\mathrm{B}})}{\partial\boldsymbol{P}}\right]^{-1} \quad (21)$$

Ranging is repeated to obtain a large number of sample orbits, simultaneously iterating the 12 interval boundary parameters and updating the reference orbital elements in order to secure the coverage of the full orbit solution space.

For Gaia, Ranging is particularly important in the case of discoveries or recoveries of objects with large ephemeris uncertainties. It promises to play a key role in the short-term linkage of Gaia observations (see below).

3. PREDICTION PROBLEM

3.1. Propagation of Probabilities

The utilization of the orbital-element p.d.f.'s constitutes a prediction problem, where additional p.d.f.'s are derived for parameters that are functions of the orbital elements. Following Muinonen and Bowell (1993), the joint p.d.f. for a given set $\boldsymbol{F} = (F_1, \ldots, F_K)^T$ of functions of orbital elements can be derived according to

$$p(\boldsymbol{F}) \quad = \quad \int d\boldsymbol{P}\, p_{\mathrm{p}}(\boldsymbol{P})\, \delta_{\mathrm{D}}(F_1 - F_1(\boldsymbol{P})) \cdot$$
$$\ldots \cdot \delta_{\mathrm{D}}(F_K - F_K(\boldsymbol{P})), \quad (22)$$

where δ_{D} is Dirac's function. In particular, the p.d.f.'s for other orbital element sets, including sets propagated to other epochs, as well as ephemerides can be established using this relationship. Ranging and VOV sampling with the subsequent propagation of the discrete sets of orbital elements provide rigorous treatments to the prediction problem.

By linearizing the arguments of Dirac's function in Equation 22 and inserting the Gaussian orbital-element p.d.f. of the linear approximation into the integral, a Gaussian p.d.f. results for the functions $\boldsymbol{F} = (F_1, \ldots, F_K)^T$ of the orbital elements. In such linearized propagation of uncertainties, the covariance matrix for $\boldsymbol{F}$ is

$$\Sigma_{\boldsymbol{F}} \quad = \quad D^T \Sigma D,$$
$$D_{jk} \quad = \quad \frac{\partial F_k}{\partial P_j},$$
$$j = 1, \ldots, 6, \quad k = 1, \ldots, K. \quad (23)$$

The orbital-element p.d.f. allows the definition of the collision probability for an individual near-Earth object in a given interval $t \in [t_-, t_+]$:

$$P_{\mathrm{c}} = \int_{V_{\mathrm{c}}} d\boldsymbol{P}\, p_{\mathrm{p}}(\boldsymbol{P}), \quad (24)$$

where the six-dimensional volume V_{c} contains those orbital elements that lead to a collision in the given interval. Evidently, extending the time interval increases the collision probability. The definition of the collision probability seems misleadingly simple: in practise, its computation can be a highly demanding task (Virtanen & Muinonen 2004, Muinonen et al. 2001).

3.2. Background for Linkage of Observations

In order to illustrate the ambiguities arising from unidentified objects and unlinked observations, consider a data base of L sets of astrometric observations of one or more objects, the number of the objects and the linkages between the sets being unknown, and consider an additional single test set of observations. For simplicity, assume that the sets are internally correctly linked and identified with a single object. There are altogether

$$L_{\mathrm{tot}} \quad = \quad \sum_{l=0}^{L} \binom{L}{l} = 2^L \quad (25)$$

different configurations (total number of combinations) for linking the test set with the L data base sets. Had the L sets been mutually exclusive, i.e., belonging to different objects, there would have been $L + 1$ configurations for linking the test set with the L data base sets. For example, assuming a small number of data base sets $L = 5$, the numbers of outcome configurations are 6 and $2^5 = 32$. For $L = 20$, the numbers are 21 and $2^{20} = 1048576$, underscoring the rapidly increasing confusion with increasing number of unlinked observations.

As yet another example relevant for massive asteroid surveys, consider two observation master sets A and B consisting of L_{A} and L_{B} sets of observations, respectively. Assume that the sets are internally correctly linked and that they are mutually exclusive. The goal is to establish the linkages from the master set A to the master set B and thus the cross-identifications of objects. The number of possible outcomes is the following finite sum:

$$L_{\mathrm{tot}} \quad = \quad \sum_{l=0}^{\min(L_{\mathrm{A}}, L_{\mathrm{B}})} l!\, \binom{L_{\mathrm{A}}}{l} \binom{L_{\mathrm{B}}}{l}. \quad (26)$$

The terms represent all possible numbers $l = 0, 1, 2, \ldots, \min(L_{\mathrm{A}}, L_{\mathrm{B}})$ of linkages between the master sets. The binomial coefficients give the numbers of possible combinations drawn from each of the two sets and the factorial $l!$ derives from the need to replace either one of the numbers of combinations by the number of permutations. The sum is symmetric and the result is independent of whether the combinations (permutations) are drawn from sets A (B) or B (A). For example, for $L_{\mathrm{A}} = L_{\mathrm{B}} = 5$

and $L_A = L_B = 10$, we obtain $L_{tot} = 1546$ and $L_{tot} = 234662231$, respectively.

For cases with $L_A = L_B$ in the example above, an analytical lower bound follows from

$$
\begin{aligned}
L_{tot} &= \sum_{l=0}^{L_A} l! \left(\begin{array}{c} L_A \\ l \end{array} \right)^2 \geq \\
&\sum_{l=0}^{L_A} \left(\begin{array}{c} L_A \\ l \end{array} \right)^2 = \left(\begin{array}{c} 2L_A \\ L_A \end{array} \right). \quad (27)
\end{aligned}
$$

3.3. Derivation of Candidate Linkages

In what follows, we concentrate on the latter example of two master sets of mutually exclusive, internally correctly linked observation sets. Clearly, the master sets give rise to $L_A L_B$ candidate inverse problems similar to that presented in Section 2. On one hand, the maximum number of true inverse problems is $L_A + L_B$, corresponding to the case where there are no linkages between the master sets and each set of observations gives rise to an inverse problem. On the other hand, the minimum number of true inverse problems is $\max(L_A, L_B)$.

One of the first goals in the practical linkage of the observation sets is the minimization of the number of candidate inverse problems to be studied in depth. Let p_{pA} and p_{pB} correspond to the orbital-element *a posteriori* p.d.f.'s for given objects in A and B, respectively. Assuming that the objects are independent, the probability for object A (B) residing in the phase-space volume V_B (V_A) of object B (A) is

$$
\begin{aligned}
P(A \in V_B) &= \int_{V_B} d\boldsymbol{P} \, p_{pA}(\boldsymbol{P}), \\
P(B \in V_A) &= \int_{V_A} d\boldsymbol{P} \, p_{pB}(\boldsymbol{P}). \quad (28)
\end{aligned}
$$

These probabilities of overlap are significant: if it is possible to certify that

$$
P(A \in V_B) \approx 0 \, , P(B \in V_A) \approx 0, \quad (29)
$$

the candidate linkage can be removed from the master list of candidate linkages.

For overlapping p.d.f.'s, the next step is to produce the p.d.f. that is the product of the two separate p.d.f.'s, with the assumption that the objects are the same so that one of the p.d.f.'s plays the role of an *a priori* p.d.f. of the other,

$$
p_{pAB}(\boldsymbol{P}) \propto p_{pA}(\boldsymbol{P}) p_{pB}(\boldsymbol{P}). \quad (30)
$$

Let V_0 be the phase-space regime of all known asteroids. After proper normalization, it is possible to compute the probability of overlap with the phase-space volume V_0 of all known objects,

$$
P(AB \in V_0) = \int_{V_0} d\boldsymbol{P} \, p_{pAB}(\boldsymbol{P}), \quad (31)
$$

If the probability is vanishingly small, the candidate linkage can again be removed from the list of candidate linkages. However, this step requires special attention as it is not desirable to throw away new kinds of objects.

The probability of overlap $P(AB \in V_0)$ allows us to give a probability score S_J for any candidate configuration J consisting of K_J candidate linkages:

$$
\begin{aligned}
S_J &= \sum_{k=1}^{K_J} P_k(AB \in V_0), \\
J &= 0, 1, 2, 3, \ldots, J_{max}, \quad (32)
\end{aligned}
$$

where J_{max} denotes the maximum number of configurations arising from the given linkage problem.

The final result is an ordered list of configurations given, for example, by the following finite sequence I:

$$
I = \{J_3, J_7, J_1, \ldots\}. \quad (33)
$$

In the case of numerous candidate configurations, the final derivation of the correct linkages and identifications is carried out via new observations.

3.4. Phase-space Address-Comparison Technique

To find possible linkages needing further analysis, we generate ephemeris clouds (R.A. and Dec.) for all objects in both sets at three common epochs, and search for overlapping ephemerides among the objects (Granvik et al. 2004). The choice of epochs can be optimized, but the use of the observational mid-epoch as the first epoch t_1 is a good first approximation. The choice can be justified based on the knowledge that the ephemeris uncertainty grows with increasing time elapsed since the last observation (Muinonen et al. 1994). The second and third ephemerides are produced by propagating orbits from the first epoch $\Delta t_2 = t_2 - t_1$ and $\Delta t_3 = t_3 - t_1$ (for example, 12 and 24 hours, respectively) forward in time, respectively, and transforming the corresponding orbital elements to ephemeris clouds. The search for similarities among the two ephemerides is carried out efficiently using the address-comparison technique (described below). Similar ephemerides at several epochs indicate a preliminary linkage, which requires further investigation using either Ranging (required for single-night linkages due to short observational arcs), VOV sampling, or differential correction of a least-squares orbit.

When searching through the bins to find overlapping ephemerides, most time is spent checking empty bins, which is inefficient. Instead of using the whole map, or multidimensional array, one can assign an address to each bin and just compare the addresses that are occupied with orbits. For example, let us study the one-dimensional discretization of a hypervolume of an N-dimensional space. Discretizing each dimension into m_n ($n = 1, 2, \ldots, N$) intervals, the total number of bins becomes

$$
N_{tot} = m_1 m_2 \cdots m_N. \quad (34)
$$

Let the N indices of a certain bin be $k_n > 0$ ($n = 1, 2, \ldots, N$). That given bin obtains an address given by the single integer

$$
\begin{aligned}
K = & \; k_1 + (k_2 - 1)m_1 + \\
& (k_3 - 1)m_1 m_2 + \ldots \\
& + (k_N - 1)m_1 m_2 \cdots m_{N-1}.
\end{aligned} \quad (35)
$$

When needed, the indices k_n can be retrieved from K via the following algorithm:

$$
\begin{aligned}
k_N &= 1 + \mathrm{int}\, \frac{K}{m_1 m_2 \cdots m_{N-1}} \\
k_{N-1} &= 1 + \mathrm{int}\, \frac{K - (k_N - 1)m_1 m_2 \cdots m_{N-1}}{m_1 m_2 \cdots m_{N-2}} \\
& \cdots \\
k_1 &= K - \sum_{n=2}^{N}(k_n - 1)m_1 m_2 \cdots m_{n-1}. \quad (36)
\end{aligned}
$$

The transformation algorithm essentially does the same as a basic binning algorithm. But instead of returning the coordinates of a bin in multidimensional space (a biproduct of the algorithm), it transforms the coordinates to a single integer K. The integer is the individual ID-number of a bin in the original multidimensional binnetwork. Among the essential input values for the transformation algorithm are the boundary values of the multidimensional space and the bin sizes. At present we take into account the whole sky, so the only essential input value is the bin size, which is currently one arcmin for both R.A. and Dec.

Because the observations of an object are inverted to a sample of orbits, and every orbit in the sample is transformed to three ephemerides and further to a value K, each object will get a one-dimensional array containing the K-values. One address thus represents the ephemerides that have been computed from a single sample orbit for all three epochs. Potential identifications are sought by comparing the K-arrays of objects in the first set with the K-arrays of objects in the second set. The search can move to the next candidate pair as soon as a single pair of equal addresses, or integers, is found.

When dealing with an array of integers, the search algorithm can be optimized more easily than when searching a multidimensional array. By sorting the K-values in ascending order, a *binary search* algorithm can be used for the search of similar elements, which significantly accelerates the comparison algorithm.

4. ORB-F95 AND ITS APPLICATION

Ranging, VOV sampling, and the least-squares method are implemented in a completely independent software bundle with Orb as the working title. Our goal is to have a state-of-the-art set of fundamental asteroid orbit computation tools that are easy to use, modify, and update. The bundle contains tools such as I/O of different observation formats, input of JPL ephemerides, coordinate and time transformations, several orbital inversion methods, differential corrections, and integration.

Different sets of orbital elements can be used during the computations, but the Cartesian elements are the basic ones. Given such a set of tools, more advanced WWW, single-processor, or multiprocessor applications for, e.g., computation of ephemerides, impact monitoring, and identification of asteroids, can be put together and maintained. The goal is achieved by using a modern programming language (Fortran 95), which allows efficient programs, dynamical memory allocation, and easy parallelization, an object-oriented programming paradigm, advanced documentation tools, and a proper error management, which greatly reduces the time spent on debugging. At present, the Orb package contains some 20 000 lines of code and the fundamental routines are in place and tested to produce correct results.

Application of Ranging to the simulated observations of two near-Earth asteroids 1993 OM_7 and 1998 OX_4 is illustrated in Figure 1, where we show the nonlinear collapse in the extent of orbital element p.d.f.'s as a function of improving observational accuracy. This phase transition effect is studied in more detail in the companion paper by Virtanen et al.

5. CONCLUSION

We have described the inverse problem assuming that the observational data consists of sky-plane positions at given epochs. For Gaia, the data will consist of both positions and motions and we are in the process of generalizing the techniques to fully accommodate motion observations. It is important to notice that the motion observations are, in the first approximation, insensitive to the effects arising from the physical characteristics of asteroids. During a single passage of the asteroid through the Gaia CCD arrays, for the vast majority of asteroids, the angular difference between the photocentre and barycentre (see Cellino et al. 2005) will be constant, allowing us to carry out accurate, unbiased orbit computations based on motion data alone.

REFERENCES

Bowell, E., Virtanen, J., Muinonen, K., Boattini, A., 2002, Asteroid orbit computation, in Asteroids III (Eds. W. Bottke et al., University of Arizona Press, Tucson, Arizona, U.S.A.) 27-43

Danby, J.M.A., 1992. Fundamentals of Celestial Mechanics, Willmann-Bell, Inc. Richmond
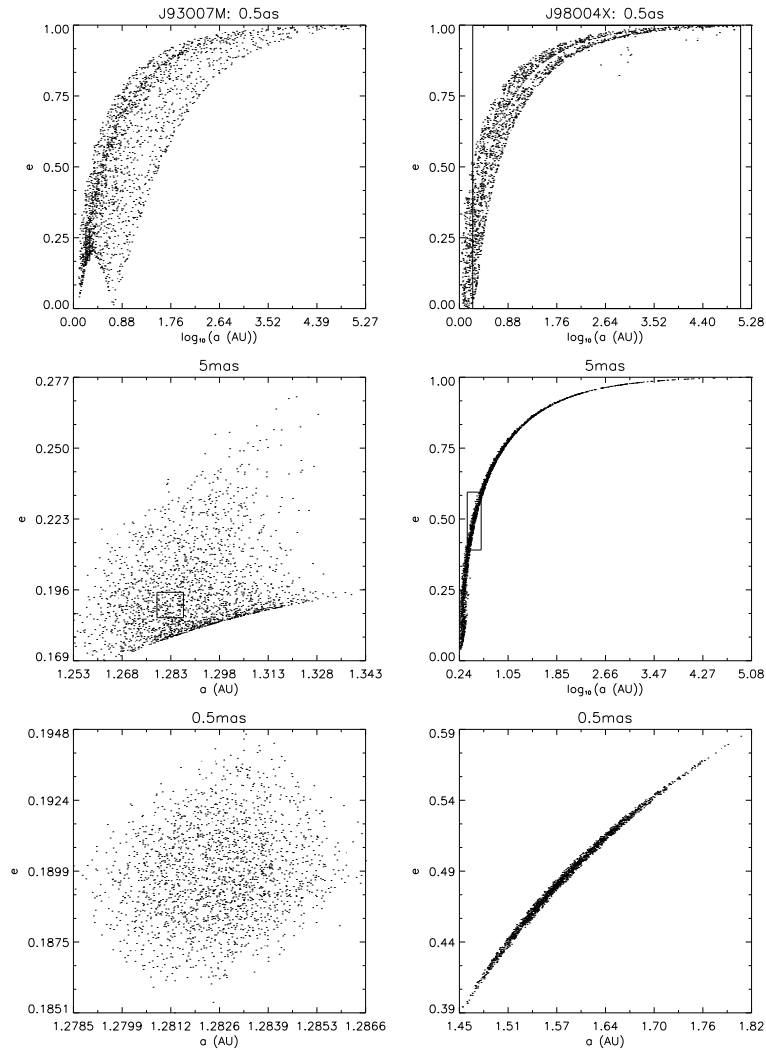
Figure 1. Nonlinear collapse in the extent of the orbital distributions with improving observational accuracy for simulated observations of near-Earth asteroids 1993 OM_7 (left) and 1998 OX_4 (right). Boxes in the four uppermost plots indicate the extents of the corresponding plotting windows below.

Granvik, M., Muinonen, K., Virtanen, J., et al., 2004, in Dynamics of Populations of Planetary Systems, Proceedings IAU Colloquium No. 197, (Z. Knezević and A. Milani, Eds.), in press

Jeffreys, H., 1946, An invariant form for the prior probability in estimation problems, Proceedings of the Royal Statistical Society of London, Series A. 186, 453-461.

Milani, A., Chesley, S. R., Chodas, P. W., Valsecchi, G. B., 2002, Asteroid close approaches: Analysis and potential impact detection, in Asteroids III (W. Bottke, R. P. Binzel, A. Cellino, P. Paolicchi, Eds., University of Arizona Press, Tucson, Arizona, U.S.A.) 55-70

Muinonen, K., 1996, Orbital covariance eigenproblem for asteroids and comets, MNRAS, 280, 1235-1238

Muinonen, K., Bowell, E., 1993, Asteroid orbit determination using Bayesian probabilities, Icarus, 104, 255-279

Muinonen, K., Bowell, E., Wasserman, L. H., 1994, Orbital uncertainties of single-apparition asteroids, Planet. Space Sci., 42, 307-313

Muinonen, K., Virtanen, J., Bowell, E., 2001, Collision probability for Earth-crossing asteroids using orbital ranging, Celestial Mechanics and Dynamical Astronomy, 81, 93-101

Muinonen, K., Virtanen, J., Granvik, M, Laakso, T., 2004, Asteroid orbits using phase-space volumes of variation, MNRAS, submitted

Press, W. H., Teukolsky, S. A., Vetterling, W. T., Flannery, B. P. 1994. Numerical Recipes in FORTRAN, The Art of Scientific Computing, Cambridge University Press

Virtanen, J., Muinonen, K., 2004, Time evolution of orbital uncertainties at discovery for the impactor candidate 2004 AS_1, Icarus, submitted

Virtanen, J., Muinonen, K., Bowell, E., 2001, Statistical ranging of asteroid orbits, Icarus, 154, 412-431

Virtanen, J., Muinonen, K., Mignard, F., 2005, ESA SP-576, this volume